Available online at www.sciencedirect.com

ScienceDirect

Ceramics International 40 (2014) 4969–4973

CERAMICS INTERNATIONAL

www.elsevier.com/locate/ceramint

Cylindrical stacks and flower-like tungsten oxide microstructures: Controllable synthesis and photocatalytic properties

Qiu-Hong Li[a], Li-Min Wang[b,*], De-Qing Chu[a], Xiao-Zhong Yang[a], Zhi-Yu Zhang[a]

[a]School of Environmental and Chemical Engineering, Tianjin Polytechnic University, Tianjin 300387, China
[b]School of Materials Science and Engineering & State Key Laboratory of Hollow-Fiber Membrane Materials and Membrane Processes, Tianjin Polytechnic University, Tianjin 300387, China

Received 2 August 2013; received in revised form 20 September 2013; accepted 25 September 2013
Available online 15 October 2013

Abstract

Cylindrical stacks WO_3 (CSWs) have been successfully prepared by the reaction of $Na_2WO_4 \cdot 2H_2O$ and HCl solution via a straightforward hydrothermal treatment in the absence of any template. And the flower-like WO_3 (FLW) microstructures have been prepared by adding polyethylene glycol (PEG-1000). The structure and property of the products were characterized by various techniques (XRD, FTIR, SEM and UV–vis). The possible formation mechanism of the two superstructures was discussed in detail according to the experimental results. In addition, the photocatalytic activities of the samples were evaluated by the degradation of methylene blue (MB). The results showed that the photocatalytic performance of FLW was more efficient compared with CSWs, demonstrating that the degradation rate may be related to their different morphologies.

Keywords: Hydrothermal; WO_3 microstructures; Photocatalytic property

1. Introduction

Micro- and nano-structures of semiconductor materials have received great interest over the past few years [1,2]. At present, controlling the synthesis of different morphologies of metal oxide has attracted considerable attention because the morphologies strongly influence their properties [3]. As one kind of important fundamental n-type semiconductors, tungsten oxide (WO_3) and its hydrates ($WO_3 \cdot nH_2O$, $n=0$–2) have been extensively researched. Numerous methods, such as template directed synthesis [4], micro-emulsion approach [5] and hydrothermal reaction, etc. [6], have been developed for the controllable preparation of particular morphologies. In order to achieve greater progress in practical application, many structurally unprecedented motifs have been discovered, including one-dimensional (1D) nanoscale building blocks (rods, wires and plates [7–9]), and other advanced shapes such as urchin-like, ribbon-like and hollow WO_3 self-assembly microstructures [10,11]. Thus, it is anticipated that other ordered super frameworks based on 1D WO_3 nanocrystals could be formed by varying the experimental conditions. However, organizing 1D nanostructure into well-defined two-dimensional (2D) or three-dimensional (3D) microstructures is still a challenge in this field.

In the present work, we have successfully synthesized CSWs by the reaction of $Na_2WO_4 \cdot 2H_2O$ and HCl solution without any assistant agents and FLW microstructures have been also obtained by the extra addition of PEG-1000 under the same hydrothermal conditions. XRD, FTIR, SEM, DRS and UV–vis were used to determine the crystal structure, morphology, and optical property. More importantly, the possible growth process for the fabricated WO_3 microstructures was expounded in detail. Furthermore, the morphology-dependent photocatalytic activities of the as-prepared WO_3 products were also tested and compared.

2. Experimental section

2.1. Chemicals

$Na_2WO_4 \cdot 2H_2O$, polyethylene glycol (PEG-1000), 36% HCl solution and absolute ethyl alcohol were used in the process as

*Corresponding author. Tel./fax: +86 22 83955762.
E-mail address: wanglimin@tjpu.edu.cn (L.-M. Wang).

0272-8842/$ - see front matter © 2013 Elsevier Ltd and Techna Group S.r.l. All rights reserved.
http://dx.doi.org/10.1016/j.ceramint.2013.09.115

raw materials. All the reagents used in the experiments were of AR grade and purchased from Kermel Co. Ltd.

2.2. Synthesis of WO_3 microstructures

In a typical method, 0.750 g $Na_2WO_4 \cdot 2H_2O$ were dissolved in 15 mL deionized water and 5 mL ethyl alcohol (solution A). Subsequently, 36% HCl solution was slowly dropped into the upper solution with stirring until the pH value reached 1.0 (solution B). Then, the solution B was transferred into a Teflon-lined autoclave and maintained at 180 °C for 24 h in an oven. After that, the product was repeatedly washed with deionized water and dried at 80 °C for 5 h. In the end, the cylindrical stacks WO_3 (CSWs) self-assembly structures were obtained after being calcination at 450 °C for 3 h. In addition, flower-like WO_3 structures (FLW) also have been synthesized through the same method by extra addition of PEG-1000 (0.250 g) into the solution A. The different hydrothermal reaction times (6, 12, 24 h) were investigated in following experiments.

2.3. Characterization

The phase and structure of products were characterized by using X-ray diffraction (XRD, D8 DISCOVER with GADDS version of BRUCK Company of Germany), Fourier transform infrared spectroscopy (FTIR, TENSOR37, BRUKER, using the potassium bromide (KBr) pellet technique), and scanning electron microscopy (SEM, Qunanta 200, FEI). The specific surface area (S_{BET}) of the samples was measured on a Micromeritics JW-BK (Beijing) analyzer and evaluated using the multipoint Brunauer–Emmett–Teller (BET) method. And the diffuse reflectance spectra were measured by a UV–vis spectrometer (TU-1901, Beijing).

2.4. Photocatalytic activities test

The photocatalytic activities of samples were evaluated by degradation of MB (100 mL, 10 mg/L) under Xenon lamp (300 W) irradiation. The initial concentration of photocatalyst was 1.0 g/L. Prior to irradiation, the suspension was stirred for 60 min in darkness to reach adsorption–desorption equilibrium. The concentration of MB during the degradation course was detected by UV–vis spectrophotometer measurement at 665 nm and the degradation rate is recorded as $(C_0–C)/C_0$, where C is the concentration of MB for each irradiated time, and C_0 is the starting concentration.

3. Results and discussion

3.1. XRD patterns and FTIR spectra

The phase of products was firstly characterized by XRD analysis. From Fig. 1a, we can observe that all of the peaks (curves (a) and (b)) can be precisely indexed to the monoclinic WO_3 (JCPDS Card no. 43-1035; $a=7.297$ Å, $b=7.539$ Å, and $c=7.688$ Å). No peaks of impurity were detected in the XRD patterns, indicating that pure WO_3 samples were prepared under the hydrothermal conditions. The strong and sharp diffraction peaks suggest that the products were of highly crystallization. Fig. 1b shows the FTIR spectra of pure WO_3 samples. The two curves are well consistent with each other, and the peak marked with arrows showed the W–O crystalline bonding vibration (803 cm^{-1}) [4].

3.2. SEM images of samples

The SEM was conducted to observe more details of morphological features of samples as shown in Fig. 2. A panoramic morphology is presented in Fig. 2a, demonstrating that a large amount of WO_3 microcrystals highly disperse in the space and take on a uniform cylindrical stacks appearance. It reveals that the well-defined cylindrical stacks 3D microstructures with diameters in the range of 2–3 μm and length of 5 μm are assembled by many densely regular nanorods (Fig. 2b). As illustrated in Fig. 2c, the flower-like WO_3 architectures have been harvested when PEG-1000 was added into the previous synthesized system. An individual image is shown in Fig. 2d, it

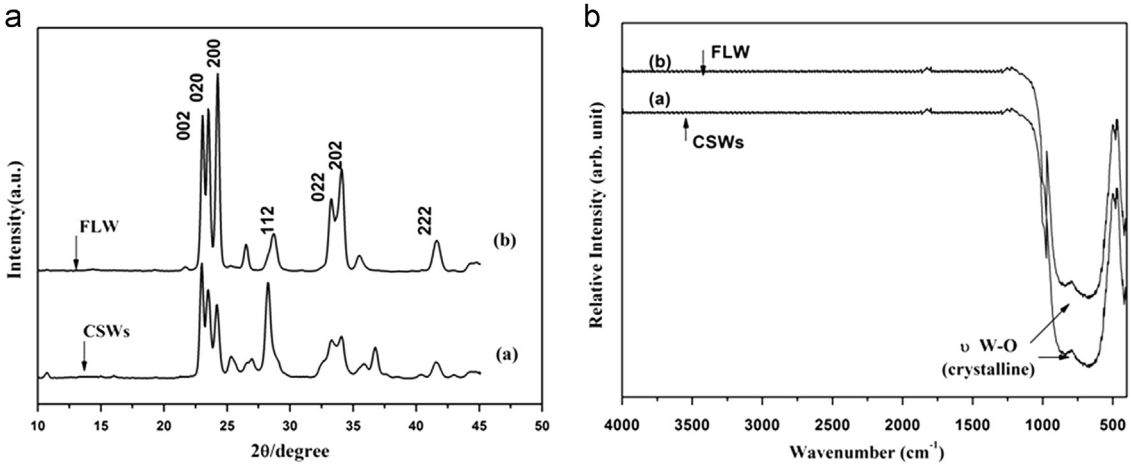

Fig. 1. XRD patterns and FTIR spectra of the as-prepared samples: CSWs (curve (a) in XRD patterns and FTIR spectra); FLW (curve (b) in XRD patterns and FTIR spectra).

can be seen that the flower-like structures are seen to visibly about the size of 4 μm. A lot of pores and ravines engendered in the 3D microstructures as described in Fig. 2d and the inset of Fig. 2b, which may improve their physical and chemical properties.

In order to deeply investigate the possible formation mechanism of the as-synthesized WO_3, the morphologies of the product at different reaction times (6, 12 and 24 h) were characterized (Fig. 3). In terms of CSWs, at the early stage (6 h), many clusters composed of nanorods are observed in Fig. 3a. Increasing the reaction time to 12 h, bigger clusters with the diameters in the range of 3–4 μm have been obtained (Fig. 3b). As revealed in Fig. 3c, the uniform CSWs finally formed when the hydrothermal reaction time was prolonged to 24 h. Furthermore, the same research method has been applied to study the growth process of FLW. At the first stage, an examination of product collected after reaction for 6 h shows that large aggregation formed by the spontaneously assembling of nanoparticals to minimize their surface energy (Fig. 3d). After reaction for 12 h, there were no significant changes on the morphology of the aggregation (Fig. 3e). Surprisingly, the FLW structures formed after conducting the reaction time for 24 h (Fig. 3f). Therefore, we can conclude that the hydrothermal reaction time is a vital factor for the final morphology.

3.3. The possible growth process

According to these experimental results, the possible growth process of the obtained structures can be proposed. In the absence of surfactant, H_2WO_4 precipitate firstly formed after 36% HCl solution was added dropwise into Na_2WO_4 solution. Then, the WO_3 crystal nucleus emerged when the reaction temperature exceeded the decomposition temperature of H_2WO_4. Subsequently,

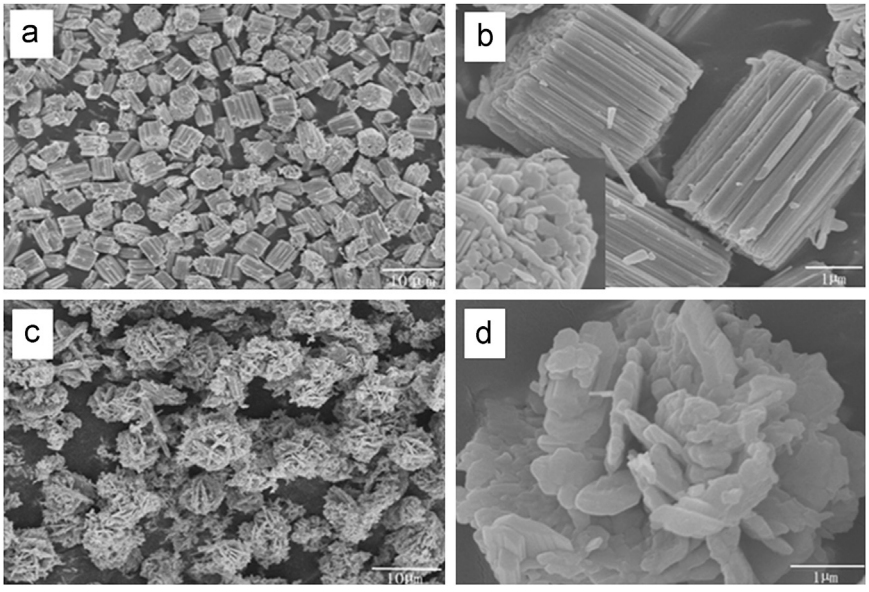

Fig. 2. SEM images of samples with reaction time for 24 h: CSWs (a and b) and FLW (c and d).

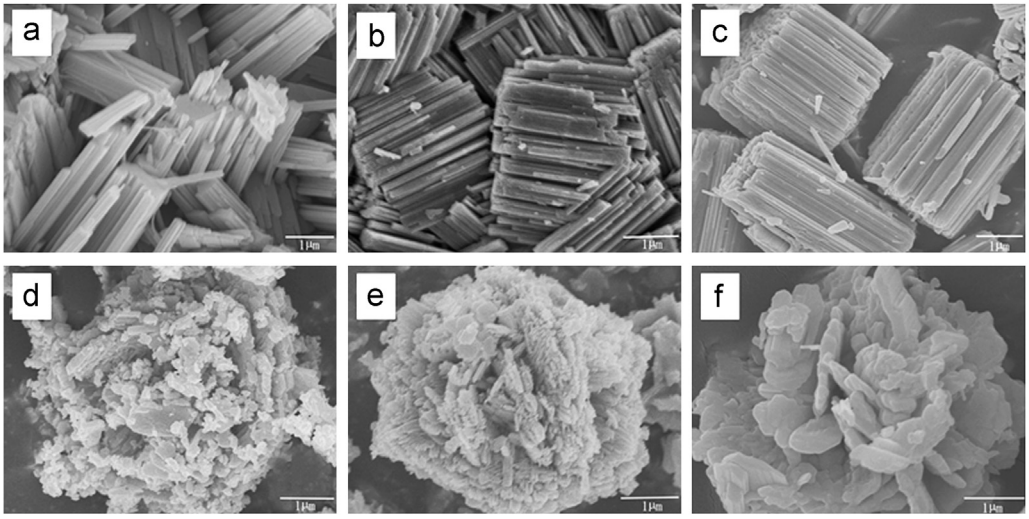

Fig. 3. SEM images of CSWs (a–c) and FLW (d and e) for different reaction times: (a–d) 6 h, (b and e) 12 h and (c–f) 24 h.

the orientated growth of WO_3 nucleus served as the most favorable factor for the growth of nanorods. Interestingly, the WO_3 nanorods assembled systematically into layer-by-layer cylindrical stacks structures with the extension of reaction time. While the addition of PEG-1000 made the formation of 3D flower-like structures. At the start of the reaction, PEG was protonated when the H^+ ions from HCl were added into the reaction solution. After that, the H^+ ions were released relatively and few primary particles may be achieved with the increase of reaction temperature. Then these particles at low concentrations should aggregate rapidly to minimize interfacial energy. In addition, PEG can inhibit the growth of some crystal faces as sealing agent. The presence of PEG could rationally control the release rate of H^+ ions and the orientation growth of WO_3 crystal nucleus, and may contribute to the well-crystallized flower-like WO_3 structures. The change of their orientation growth is believed to be the key factor of the morphology evolution. As it is reported that the oriented-attachment mechanism originally put forward by Penn and Banfield has been applied to explain the growth of various oriented and hierarchical nanostructures via self-assembly of nanocrystals [10]. According to the above analysis, it can be inferred that the self-assembly and oriented-attachment mechanisms may be responsible for the two different growth processes. The possible schematic reaction mechanism of the synthesized WO_3 is depicted in Fig. 4.

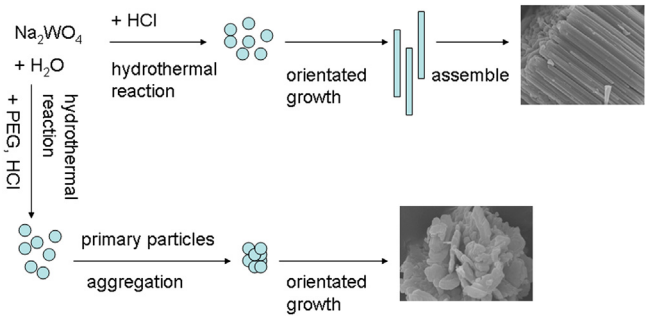

Fig. 4. Schematic illustration for the possible formation mechanism of synthesized WO_3.

3.4. The photocatalytic properties investigate

Fig. 5a presents the UV–vis diffuse reflectance spectra of WO_3 samples. The band gap can be calculated by the following equation [12] $(\alpha h\nu)^{1/2}=K(h\nu-E_g)$ where α, ν, E_g and K are the absorption coefficient, incident photon energy, band gap and constant, respectively. The insets in Fig. 5 show the plot of $(\alpha h\nu)^{1/2}$ versus $h\nu$. The band gaps of the CSWs and FLW are about 2.58 eV and 2.55 eV, respectively, by extrapolating the linear plots [12]. These values are lower than that of WO_3 as reported early, such as hierarchical WO_3 spheres owned a band gap value of 2.68 eV, 2.62 eV for dumbbells and 2.60 eV for commercial particles calculated from the absorption insets [13].

The photocatalytic activities of the WO_3 were examined by the degradation of MB solution, and the results were shown in Fig. 5b. When the suspension was stirred for 60 min in darkness, the system had reached adsorption–desorption equilibrium. The blank experiment shows that the degradation of MB is extremely slow without photocatalyst. After illumination by visible light for 60 min, the degradation rates approached to 94.7% (FLW) and 90.3% (CSWs). The results indicated that the photocatalytic activity of FLW was more efficient than CSWs. The high photocatalytic performance of our products may be attributed to their high BET surface area. S_{BET} is 121.8 $m^2\,g^{-1}$ for FLW, and it is107.31 $m^2\,g^{-1}$ for CSWs. Furthermore, their hierarchical structures are also important influenced factors for the high photocatalytic performance [14].

4. Conclusions

In summary, we demonstrate a low cost and typical hydrothermal process for fabricating well-aligned cylindrical stacks and flower-like WO_3 microstructures. Based on time-dependent experiments, we conjecture that the self-assembly and oriented-attachment mechanism are benefit for the formation of WO_3 microstructures. And it can be conclude that the PEG is an important factor that influences WO_3 crystal growth in the process of reaction. In addition, the photocatalytic activity experimental results indicated that the degradation

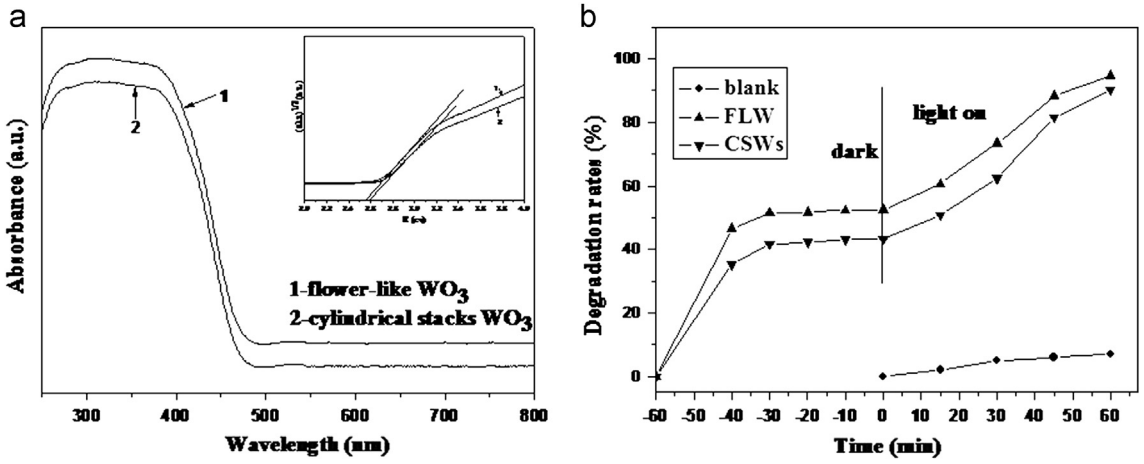

Fig. 5. (a) UV–vis diffuse reflectance spectra (DRS) of samples; inset is the calculation diagram of their band gaps and (b) photocatalytic degradation rates of as-prepared WO_3.

rates of the FLW and CSWs were 94.7% and 90.3%, which may be close related to the band gap values (2.55 eV and 2.58 eV) affected by their different morphologies probably. At the same time, our experiments demonstrate that the surface area of the catalysts have great influence on their photocatalytic activity.

References

[1] T.R. Gordon, M. Cargnello, T. Paik, F. Mangolini, R.T. Weber, P. Fornasiero, et al., Nonaqueous synthesis of TiO_2 nanocrystals using TiF_4 to engineer morphology, oxygen vacancy concentration, and photocatalytic activity, J. Am. Chem. Soc. 134 (2012) 6751–6761.

[2] K. Lv, J. Li, X. Qing, W. Li, Q. Chen, Synthesis and photo-degradation application ofWO_3/TiO_2 hollow spheres, J. Hazard. Mater. 189 (2011) 329–335.

[3] Y.J. Zhang, Or S.W., X. Wang, T. Cui, W. Cui, Y. Zhang, et al., Hydrothermal synthesis of three-dimensional hierarchical CuO butterfly-like architectures, Eur. J. Inorg. Chem. (2009) 168–173.

[4] C.C. Chena, C.H. Cheng, C.K. Lin, Template assisted fabrication of TiO_2 and WO_3 nanotubes, Ceram. Int. 39 (2013) 6631–6636.

[5] N. Asim, S. Radiman, M.A. Yarmo, Synthesis of WO_3 in nanoscale with the usage of sucrose estermicroemulsion and CTAB micelle solution, Mater. Lett. 61 (2007) 2652–2657.

[6] J.Y. Li, J.F. Huang, J.P. Wu, L.Y. Cao, Y. Kazumichi, Morphology-controlled synthesis of tungsten oxide hydrates crystallites via a facile, additive-free hydrothermal process, Ceram. Int. 38 (2012) 4495–4500.

[7] F. Zheng, M. Zhang, M. Guo, Controllable preparation of WO_3 nanorod arrays by hydrothermal method, Thin Solid Films 534 (2013) 45–53.

[8] K. Jarmo, M. Melinda, L. Anne-Riikka, M. Jani, H. Niina, S. Andrey, et al., Room temperature hydrogen sensors based on metal decorated WO_3 nanowires, Sens. Actuators B 186 (2013) 90–95.

[9] J. Sungpanich, T. Thongtemb, S. Thongtem, Large-scale synthesis of WO_3 nanoplates by a microwave-hydrothermal method, Ceram. Int. 38 (2012) 1051–1055.

[10] Z.J. Gu, T. Zhai, B. Gao, X. Sheng, Y. Wang, H. Fu, et al., Controllable assembly of WO_3 nanorods/nanowires into hierarchical nanostructures, J. Phys. Chem. B 110 (2006) 23829–23836.

[11] J. Liu, M. Sasidharan, D. Liu, Y. Yokoyama, S. Yusa, K. Nakashima, Novel MoO_3 and WO_3 hollow nanospheres assembled with polymeric micelles, Mater. Lett. 66 (2012) 25–28.

[12] J.H. Huang, L. Xiao, X.L. Yang, WO_3 nanoplates, hierarchical flower-like assemblies and their photocatalytic properties, Mater. Res. Bull. 48 (2013) 2782–2785.

[13] J.F. Yin, H.Q. Cao, J.X. Zhang, M. Qu, Z. Zhou, Synthesis and applications of γ-tungsten oxide hierarchical nanostructures, Cryst. Growth Des. 13 (2013) 759–769.

[14] J.Z. Su, X.J. Feng, J.D. Sloppy, L.J. Guo, C.A. Grimes, Vertically aligned WO_3 nanowire arrays grown directly on transparent conducting oxide coated glass: synthesis and photoelectrochemical properties, Nano Lett. 11 (2011) 203–208.